

Boundary-induced nucleation control: A theoretical perspective

Oleg Buller^{1,*}, Hong Wang², Wenchong Wang², Lifeng Chi^{2,3}, and Andreas Heuer¹

¹ *Institut für Physikalische Chemie, Universität Münster, 48149 Münster, Germany*

² *Physikalisches Institut and Center for Nanotechnology (CeNTech),
Universität Münster, 48149 Münster, Germany and*

³ *Jiangsu Key Laboratory for Carbon-based Functional Materials & Devices Collaborative,
Institute of Functional Nano & Soft Materials (FUNSOM) and
Collaborative Innovation Center of Suzhou Nano Science and Technology,
Soochow University, Suzhou 215123, P. R. China*

The pre-patterning of a substrate to create more attractive or repulsive regions allows one to generate a variety of structures in vapor deposition experiments, specific of technological relevant semiconducting organic molecules. A particular interesting structure is generated if the attractive region is forming a rectangular grid. For specific combinations of the particle flux, the substrate temperature and the lattice size it is possible to generate exactly one cluster per cell, giving rise to nucleation control. Here we show that the experimental observations of nucleation control can be very well understood from a theoretical perspective. For this purpose we perform, on the one hand, kinetic Monte Carlo simulations and, on the other hand, use scaling arguments to rationalize the observed behavior. For several observables, characterizing nucleation control, we find a very good agreement between experiment and theory.

PACS numbers: 61.66.Hg, 68.55.A-, 81.15.-z, 85.40.Hp

Keywords: organic molecules, surface diffusion, aggregate, nucleation

I. INTRODUCTION

With physical vapor deposition (PVD) material can be condensed onto a substrate [1], yielding films with desired thickness [2, 3]. One key application is organic electronics e.g. semiconducting organic molecules have a great potential in microelectronics in terms of functionality and efficiency [4, 5].

To understand the mechanisms on the surface after PVD one has to take into account mainly the diffusion and the nucleation processes. For a nucleation process a critical number of molecules has to come together to form stable clusters [2, 6–9]. By using different molecules one can even perform colour tuning with the simultaneous use of different molecules [10–13].

In [14] we have introduced a new approach to generate regular molecular clusters by an appropriate choice of a pre-patterned substrate. The clusters directly grow on the substrate and not only on the pre-pattern, which is energetically more favorable. In the interpretation, put forward in [14], it is shown, that the randomness of the nucleation can be controlled without using defects in form of gold aggregates or step edges, by preparing the particle density in an confined area. Using adsorbing boundaries, lead to a parabolic like deposited particle density profile including a maximum in the center of the cell. This property is independent from the structure of the deposited molecules, as shown by experiments and simulations [14]. In order to elucidate the mechanism behind this formation, we use a lattice based kinetic Monte Carlo model [15–19].

The goal of the present work is twofold. First, we

present a quantitative comparison between the simulation and the experimental results for different observables which characterize properties of the clusters and in particular the nucleation control, i.e. the presents of exactly one cluster per cell. Second, we analyse the dependence on the external flux of molecules, based on analytical calculations, kinetic Monte Carlo simulations and experiments.

The structure of this paper is as follows. In Sect. II we give an insight into the experimental results of cluster formation followed by the simulations setup in Sect. III. Afterwards we discuss the qualitative behavior of cluster growth in Sect. IV and the theory of single-cluster formation Sect. V. Nucleation- and position control is discussed in Sect. VI. The flux dependence of the nucleation control is presented in Sect. VII, the influence of the diffusion properties in Sect. VIII. Finally, we conclude with a discussion of our results in Sect. IX.

II. EXPERIMENTAL BACKGROUND

In the experiment the functional molecule N, N'-bis(1-naphthyl)- N, N'-diphenyl-1,1'-biphenyl'-4,4'-diamine (NPB, a molecule widely used for organic light emitting diodes), has been used [20]. This molecule was deposited on a silica surface. To create an attractive region for the molecules, a gold grid was put on the surface by standard beam lithography [10]. The gold grid is acting as an adsorbing environment for the central area of the squares. More details can be found in [14].

In Fig. 1 we show the scanning electron microscope of the resulting structure for a gold array distance of 4.0 μm . The flux was increased going from left to right. In case of the lowest flux $F = 0.042 \text{ nm/s}$, shown in Fig. 1 left, one cluster is created with a well-defined position in the

* To whom correspondence should be addressed: o.buller@www.de

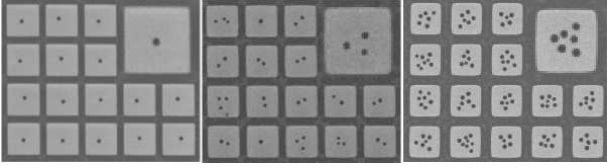


FIG. 1. SEM pictures from the experiment for $L = 4.0 \mu\text{m}$ and flux variation 0.042 nm/s, 0.066 nm/s, 0.085 nm/s from left to right.

center of the cell. Due to the regularity of the grid the clusters also form a regular structure. With increasing the flux the number of clusters increases, i.e. nucleation control is no longer present.

III. SIMULATION SETUP

We use a three dimensional cubic lattice model with a lattice constant of a . It is the same model as described in [14]. Every lattice site $i = \{i_x, i_y\}$ can be occupied by three different particle types: deposited particles p_i , substrate particles s_i and the more attractive pre-pattern particle g_i (in the experiment represented by gold). The lattice site i is either filled or empty. As we are only interested in the dynamics of the deposited particles the Hamiltonian can be written as

$$H = -\varepsilon_{pp} \frac{1}{2} \sum_{i,j} f(r_{ij}) p_i p_j - \varepsilon_{pg} \frac{1}{2} \sum_{i,j} f(r_{ij}) p_i g_j - \varepsilon_{ps} \frac{1}{2} \sum_{i,j} f(r_{ij}) p_i s_j, \quad (1)$$

where the ε_{xy} ($x, y \in \{p, g, s\}$) are the interaction parameters. $f(r_{ij})$ depends on the distance r_{ij} between the particles on position i and j and represents the distance scaling function. It is defined as follows:

r_{ij}	0.0	1.0	$\sqrt{2}$	$\sqrt{3}$	$> \sqrt{3}$
$f(r_{ij})$	0.0	1.0	1.0	0.5	0.0

As in previous work [21] the interaction up to the third nearest neighbors (common corner) is taken into account. We use one cell with the more attractive environment as our simulation box with periodic boundary conditions in the substrate plane (x - and y - direction); see Fig. 2.

Simulations are done for different cell sizes L and a fixed stripe width of $20a$. The substrate is composed of one layer including pre-pattern and substrate particles, which are fixed during the simulation. The simulation starts with a particle-free substrate. During one Monte Carlo (MC) step, corresponding to the time step Δt , every particle on the substrate attempts one 3D nearest-neighbor move. It is accepted according to the standard Metropolis criterion [22]. Furthermore, all moves are discarded after which a particle has zero energy. In this way possible desorption processes are suppressed. After finishing the MC step, n particles are added to the system.

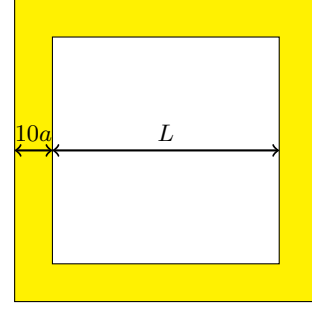


FIG. 2. Sketch of the simulation box.

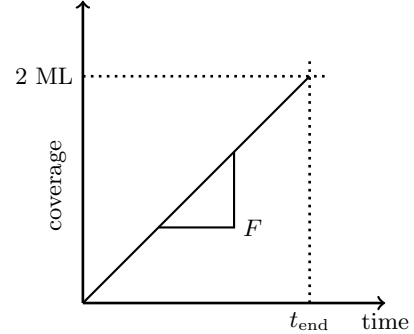


FIG. 3. Simulation time scale.

n is a Poissonian random number with the mean value \bar{n} , which is related to the average flux via

$$F = \frac{\bar{n}}{(A\Delta t)}. \quad (2)$$

Here, $A = (L + 20a)^2$ is defined as the surface area. The added particles are directly attached on a randomly chosen free position of the surface. The resulting time-dependence of the coverage (number of particles over A) is sketched in Fig. 3.

All simulations are repeated 2000 times in order to obtain a good statistical description. This large number also acknowledges that the nucleation process have a significant random component which has to be appropriately averaged out.

IV. GROWTH OF CLUSTER - QUALITATIVE BEHAVIOR

Our key observable is the average number of clusters in the cell $\langle N \rangle$. As already shown in [14], via variation of L for constant flux the value $\langle N \rangle$ can be tuned. For very small values of L most particles are finally adsorbed at the pre-pattern boundaries and no cluster can form. In contrast, for very large L the boundary only plays a minor role and standard nucleation behavior can be observed [23]. Of particular interest is the single L value for which $\langle N \rangle$ is unity, i.e. on average a single cluster is formed per cell. In practice we tune the chosen flux for fixed L , until $\langle N \rangle \approx 1$.

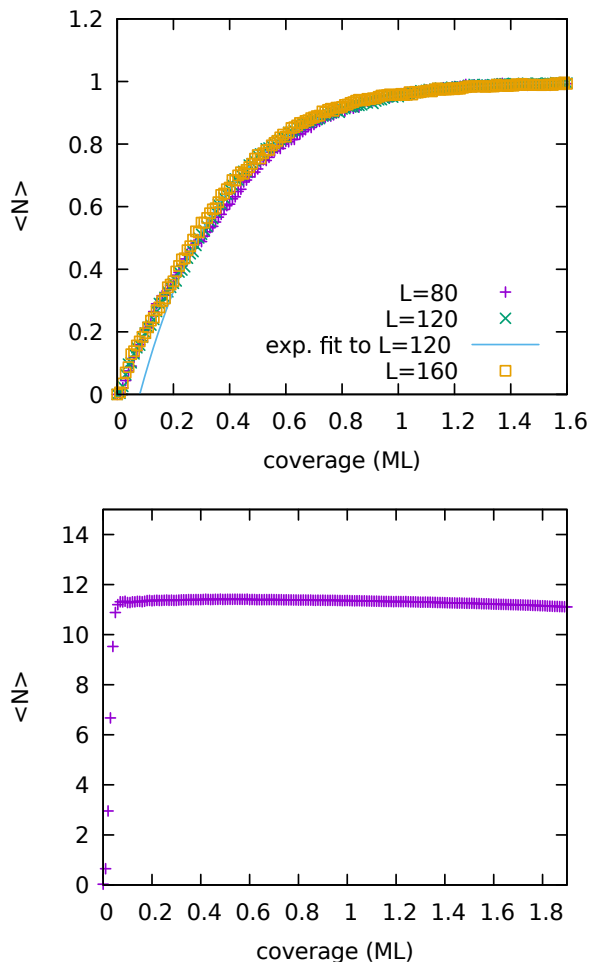


FIG. 4. Average number of clusters in dependence of the coverage. For $L = 120$ an exponential fit to the long-time behavior is included. (Top) Simulations for different L values. The respective values for the corresponding flux values are listed in Tab.I. (Bottom) Simulations for $F = 5.8 \times 10^{-6}/(a^2 \Delta t)$ and $L = 160$.

TABLE I. Data for $\langle N \rangle = 1$ with cell size L the corresponding flux F , the average cluster number $\langle N \rangle$ the corresponding standard deviation σ , and yield (fraction of cells with exactly one cluster).

L/a	F in $10^{-6}/(a^2 \Delta t)$	$\langle N \rangle$	σ	yield in %
40	36.11	1.014	0.205	95.8
60	12.03	1.004	0.228	94.8
80	5.80	1.008	0.222	95.1
120	2.14	0.987	0.238	94.3
160	1.08	0.996	0.217	95.3

Strictly speaking the value of $\langle N \rangle$ depends on the coverage of the surface. In Fig. 4 (top) the diagram $\langle N \rangle$ against the coverage in monolayer (ML number of particles per full surface coverage) is shown for different values of L . The respective values for the corresponding flux values are listed in Tab.I. Interestingly, when expressing the time in terms of the coverage, one observes no ma-

jor dependence on the length or the flux, respectively. As a consequence the doubling of the flux gives rise to a doubling of the nucleation rate under the condition of an appropriate choice of the new length to guarantee $\langle N \rangle = 1$.

The exponential fit, also shown in Fig. 4 (top), works quite well for a coverage larger than 0.2 ML. In this regime the nucleation rate is independent of time. Note that in the long-time regime for a coverage over 1.5 ML the value of $\langle N \rangle$ reaches a plateau, i.e. no new clusters are formed. Of course, the individual clusters are still growing. As a consequence, the value of $\langle N \rangle$, determined for a coverage of 2.0 ML, is very well defined and insensitive on the chosen coverage. The exponential fit does not work for low coverage. A detailed analysis of the short-time behavior, however, is beyond the scope of this work.

In contrast, for $F = 5.8 \times 10^{-6}/(a^2 \Delta t)$ and $L = 160$ on average more than 11 clusters are created per cell; see Fig. 4 (bottom). Almost all nucleation proceeds before 0.1 ML are deposited. The curve displays a maximum at 0.4 ML and slightly decreases for longer times, indicating some coarsening effect which, however is small.

V. THEORY OF SINGLE-CLUSTER FORMATION

V.1. Existence of a critical density

Here we repeat the recently published [14] key ideas to understand the effect of varying the grid the length L for fixed flux F . For an individual simulation run we always restrict ourselves to times before a cluster forms. This helps us to capture the conditions for the formation of the first cluster.

We start by considering the particle density distribution $\rho(x, y, t)$ under the condition that no nucleation has occurred until time t , i.e. no increase of the local density due to nucleation occurs. Thus we can apply a continuum approach based on Burton-Cabrera-Frank theory for the case of complete condensation [24–26]

$$\frac{\partial}{\partial t} \rho(x, y, t) = D \Delta \rho(x, y, t) + F. \quad (3)$$

The pre-pattern grid acts as an adsorbing boundary, written as

$$\rho(x = 0, L, y, t) = \rho(x, y = 0, L, t) = 0. \quad (4)$$

The solution for the stationary regime $\frac{\partial}{\partial t} \rho(x, y, t) = 0$ can be expressed in terms of a Fourier series. We get

$$\rho_{\text{stat}}(x, y) = \sum_{m, n \text{ odd}} A_{m, n} \frac{FL^2}{D} \sin\left(\frac{m\pi x}{L}\right) \sin\left(\frac{n\pi y}{L}\right) \quad (5)$$

with the numerical value $A_{m, n} = 16/(\pi^4 mn(m^2 + n^2))$. Note that $\rho_{\text{stat}}(x, y)$ is dominated by the single term

$m = n = 1$ for which $\rho_{\text{stat}}(x, y)$ displays a significant maximum in the center of the cell. The density $\rho^* \equiv \rho_{\text{stat}}(x = L/2, y = L/2)$ at this maximum reads

$$\rho^* = \sum_{m, n \text{ odd}} A_{n, m} \frac{FL^2}{D} \sin\left(\frac{m\pi}{2}\right) \sin\left(\frac{n\pi}{2}\right). \quad (6)$$

To obtain a density $\rho(x, y, t)$ from the simulation results we use the projection of the three-dimensional deposited particle distribution onto the surface plane $P(x_i, y_j)$. If the position (x_i, y_j) is occupied by a deposited particle we choose $P(x_i, y_j) = 1$, otherwise $P(x_i, y_j) = 0$. The density $\rho(x_i, y_j)$ is then defined as the ensemble average of $P(x_i, y_j)$, i.e.

$$\rho(x_i, y_j) = \langle P(x_i, y_j) \rangle. \quad (7)$$

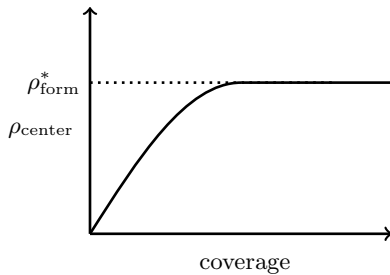


FIG. 5. Increase of $\rho_{\text{center}} = \rho(x = L/2, y = L/2, t)$ with coverage for $\langle N \rangle = 1$ in the cluster-free subensemble. The long-limit of ρ_{center} , denoted ρ^* , defines the value of ρ_{form}^* .

In Ref.[14] the time-dependence of $\rho(x = L/2, y = L/2, t)$, obtained from simulations, has been analyzed in detail. Note again, that only those realizations contribute for which until time t no nucleation process has occurred (*cluster-free subensemble*). For the interesting case $\langle N \rangle = 1$ a sketch of the time-dependence is shown in Fig. 5. Its long-time limit agrees very well with the calculated value of ρ^* ; see Eq. 6. We denote this value by ρ_{form}^* . It has an important interpretation when interpreting simulations with a different value of L . For smaller L , implying $\rho^* < \rho_{\text{form}}^*$ cluster formation is strongly suppressed, i.e. $\langle N \rangle < 1$. In contrast, in the opposite limit many clusters start to grow as soon as $\rho(x = L/2, y = L/2, t)$ approaches ρ_{form}^* . Thus, the stationary regime is never reached because of preceding nucleation events. As a consequence ρ_{form}^* can be interpreted as the density where nucleation suddenly sets in. Since the nucleation rate scales with a high power of the density (depending on the size of the critical nucleus), this observation is not surprising.

As a consequence of this interpretation it comes out quite natural that for $\langle N \rangle = 1$ the nucleation process occurs close to the center of the cell; see Fig. 1, since only for a small spatial regime one has $\rho(x = L/2, y = L/2, t) \approx \rho_{\text{form}}^*$.

V.2. Flux-dependence of the critical density

On a purely theoretical basis one can estimate the flux-dependence of the critical density ρ_{form}^* . According to standard nucleation theory [23] the local nucleation rate scales like $\Gamma_{\text{loc}} \propto \rho^{I+1}$ if I denotes the critical nucleation size. Note that in Eq. 5 the spatial dependence is given by x/L and y/L , respectively. As a consequence, the spatial range close to the center, where cluster formation can occur, i.e. $\rho_{\text{stat}}(x, y) \approx \rho_{\text{form}}^*$, is proportional to the total area L^2 . Thus, for the interesting case $\langle N \rangle = 1$ one obtains for the total nucleation rate

$$\Gamma_{\text{tot}} \propto \rho_{\text{form}}^{*I+1}(F)L^2. \quad (8)$$

The possible flux-dependence is explicitly indicated. Of course, this relation only holds under the condition that no nucleation has occurred so far.

As observed in Fig. 4 the growth of nuclei, if plotted against the coverage, does not depend on the flux. As an immediate consequence one has the simple scaling $\Gamma_{\text{tot}} \propto F$, i.e. when doubling the flux and appropriately modifying the length L to keep $\langle N \rangle = 1$ also the total nucleation rate will become twice as large. From Eq. 6 it follows that there is a direct relation between the chosen length scale L and the flux F . Choosing $L^2 \propto \rho_{\text{form}}^*(F)/F$ one explicitly keeps track of the flux dependence in order to keep $\rho^* \equiv \rho_{\text{stat}}$ constant. Inserting both relations into Eq. 8 one gets $F \propto \rho_{\text{form}}^{*I+2}(F)/F$ and thus

$$\rho_{\text{form}}^*(F) \propto F^p \quad (9)$$

with $p = 2/(I+2)$ as an immediate consequence one can predict how one has to vary the grid size L in order to keep $\langle N \rangle = 1$ when varying the flux. In general Eq. 6 yields $L^2 F \propto \rho_{\text{form}}^*(F)$. Together with Eq. 9 this yields

$$L \propto F^{-q} \quad (10)$$

with

$$q = \frac{1-p}{2} = \frac{I}{2(I+2)}. \quad (11)$$

As a matter of fact we end up with the same argumentation given by Rangelov *et al.* [27], who used a similar ansatz to analyse the island creation on stepped surfaces. The resulting scaling exponent of $p = I/(2(I+2))$ is in accordance with island density scaling, one would expect on homogeneous substrate for complete condensation [28].

VI. NUCLEATION AND POSITION CONTROL

One experimental goal is to generate a structure where ideally in every cell there is exactly one cluster which, furthermore, is located directly in the center of the cell. This would correspond to ideal nucleation and position control, respectively. In what follows we compare the nucleation and position control from the simulations with the experiments. We always consider the case $\langle N \rangle = 1$.

First, to check the quality of nucleation we determined the standard deviation of $\langle N \rangle$, which is shown in Fig. 6. It turns out that the quality of the nucleation control

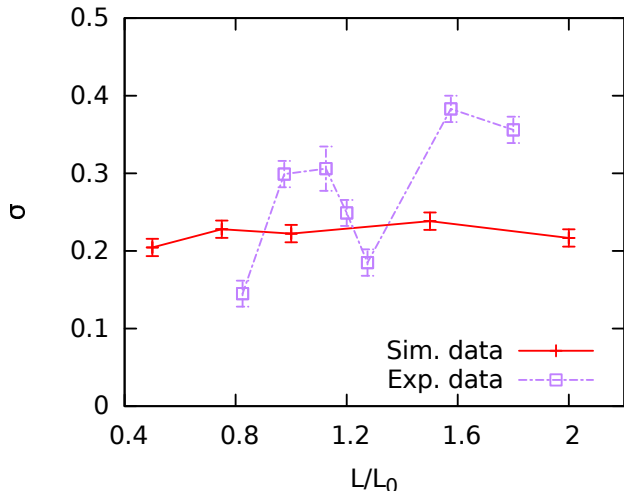


FIG. 6. Standard deviation of $\langle N \rangle$ from experiment and simulation. In simulation data $L_0 = 80a$ and for experimental data $L_0 = 0.375 \mu\text{m}$

from the simulations is independent of the chosen (F, L) -pair. A standard deviation of 0.2 together with an average value of unity means that in approx. 95% of all cells there is indeed a single cluster, compare Table I, whereas in the remaining cells there is the same number of cells with no or two cluster. The independence from L just reflects the scaling properties, discussed above. Thus, after rescaling the time- and length scale the nucleation behavior is basically identical.

It is very promising that the standard deviations, seen experimentally, are very close to the simulated ones. This shows that indeed the lattice model represents the key properties of the nucleation behavior of the actual molecules. The fluctuations as a function of L are much larger than expected from statistical reasons. Experimentally, reasons for fluctuation of experimental data could be related to a slightly uncontrolled coverage and contamination on the substrates.

Second, to analyse the position control we identify for each cluster the center of mass and then analyse the spatial distribution of these centers. Naturally, this distribution has its maximum in the middle of the cell. In the next step we determine the full width at half maximum (FWHM). Due to the scaling arguments, already discussed above, we expect that this width should scale with L . Indeed, as shown in Fig. 7, the ratio FWHM/L is independent of L . Again, simulations and experiments basically displays the same values. Furthermore this ratio is quite small which is a quantitative confirmation that not only nucleation control but also position control works very well.

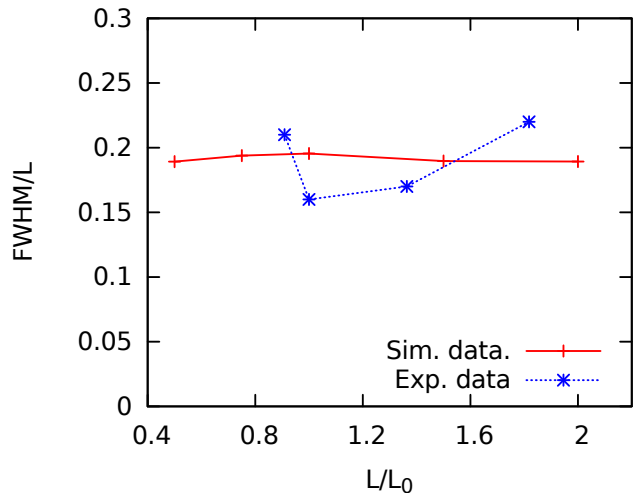


FIG. 7. Full width at half maximum of the center of mass distribution corresponding to the center of the cell $(L/2, L/2)$ scaled by the cell size L .

VII. FLUX DEPENDENCE

As discussed in Sect. V.2 the key observable to characterize the underlying flux dependence of the cluster formation is the observable ρ_{form}^* . We have determined its value for different (F, L) -pairs, corresponding to $\langle N \rangle = 1$ as given in Table I. Note that according to Fig. 5 the simulated density ρ_{form}^* can be determined from the stationary long-time regime under the condition $\langle N \rangle = 1$. The extracted ρ_{form}^* values are shown in Fig. 8.

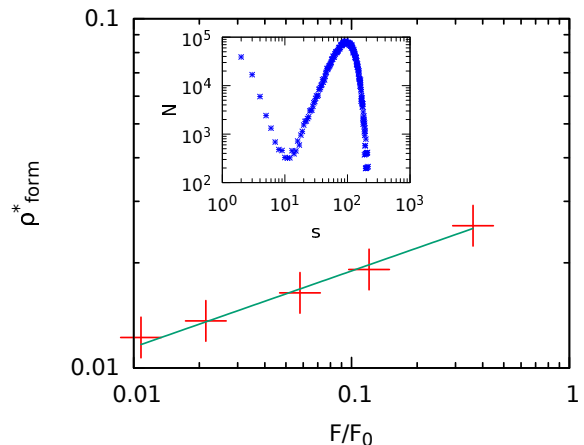


FIG. 8. ρ_{form}^* against F/F_0 ($F_0 = 10^4 \frac{1}{\sigma^2 \Delta t}$) for appropriately chosen cell sizes, corresponding to $\langle N \rangle = 1$. Included is a power law fit with an exponent of 0.25. In the inset the histogram of cluster sizes s is shown which is observed from simulations on un-patterned substrates. The minimum is found for $s = 10$.

Indeed, as expected from Eq. 9 we observe a power-

law relation between ρ_{form}^* and F with an exponent of $p = 0.25$. In Eq. 9 this exponent is expressed in terms of the critical cluster size I . We estimate the value of I by analysing the distribution of cluster sizes for a simulation on an un-patterned substrate. The minimum can be taken as a measure for I [29]. In this way we obtain $I = 10$. According to Eq. 9 this would give rise to an exponent of 0.17 which is very close to the observed value of 0.25.

In the next step we can predict the dependence of the system size on the flux. As discussed in Sect V.2 the slope should be given by $q = (1 - p)/2 = 0.38$. Indeed, the simulated data can be described very well by this exponent, see Fig. 9 top.

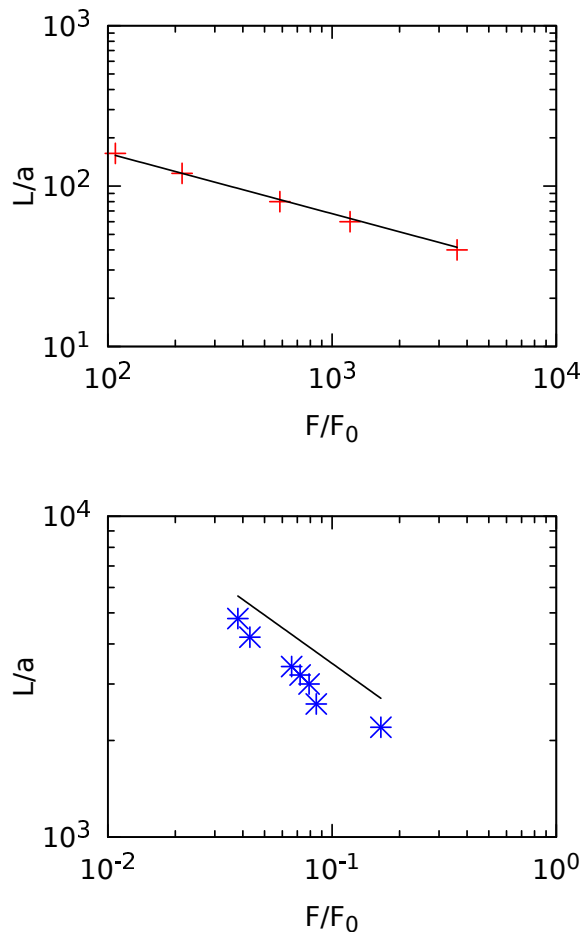


FIG. 9. F/F_0 against L for $\langle N \rangle = 1$. (top) Simulation data. Included is a power law graph with an exponent of $q = 0.38$. $F_0 = 10^8/(a^2 \Delta t)$. (bottom) Experimental data with F in units of nm/s. In this case the value of L is expressed in units of the elementary length scale of the organic molecule which it approximated as $a = 1$ nm. Included is a power-law with exponent $q = 0.5$.

For studying the experimental $F(L)$ -dependence we obtain on exponent $q \approx 0.5$, compare Fig. 9 bottom. Due to the fact of unknown condensation mechanism in the experiment, which determines the scaling of $L(F)$

[28], we can not determine the exact critical cluster size. Nonetheless this shows that the scaling in general is not limited to a specific regime of condensation.

VIII. SCALING: FROM NUCLEATION CONTROL TO STANDARD NUCLEATION

VIII.1. F/D -scaling

It is known from nucleation theory that the number of clusters in the stationary long time limit on a plain substrate is a function of F/D where D is the diffusion constant [23]. In the present case this would correspond to the limit of large $\langle N \rangle$ where the influence of the boundaries hardly matter. From our theoretical approach to nucleation control (Eq. 6) we also expect a perfect F/D scaling for $\langle N \rangle = 1$.

Here we check whether this scaling with F/D indeed holds for the large range of $\langle N \rangle$ -values. For this purpose we vary the values of D and F individually. Specifically, we introduce a diffusion parameter D as the probability to make a MC move. Therefore $D \in [0, 1]$ for $D = 1.0$ we have MC dynamic as before, for $D = 0.5$ every second try for a MC step is denied, for $D = 0.0$ the system does not move at all. Thus, for decreasing D the dynamics in the system is slowed down. In Fig. 10 we show the average number of stable clusters $\langle N \rangle$ against D/F . Note that

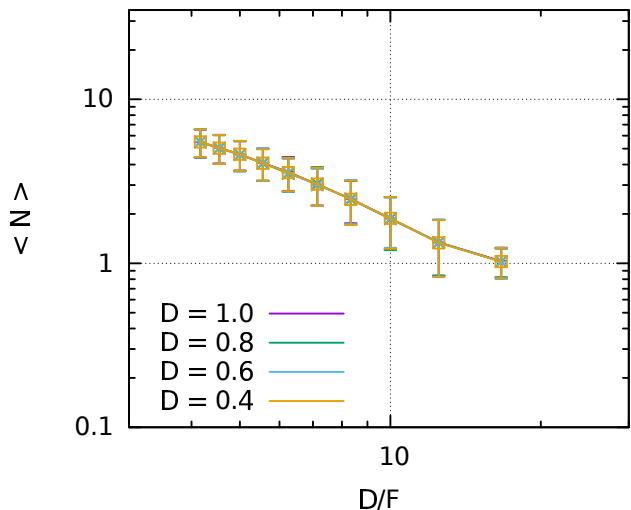


FIG. 10. Average number of clusters versus D/F for different values of the diffusion parameter as indicated in the figure and the corresponding flux F . The flux is scaled by factor 10^4 .

a perfect scaling is observed for all values of $\langle N \rangle$. As a practical consequence, we can always choose $D = 1.0$ in order to optimize the efficiency of the MC simulations but nevertheless cover all possible diffusion constants.

VIII.2. Impact of length L

Finally we look at the scaling of $\langle N \rangle$ for a fixed flux $F = 5.8 \times 10^{-6}/(a^2 \Delta t)$ and different cell sizes L following the experimental results in Fig. 1. The data is shown in Fig. 11. Is it possible to judge from which system size

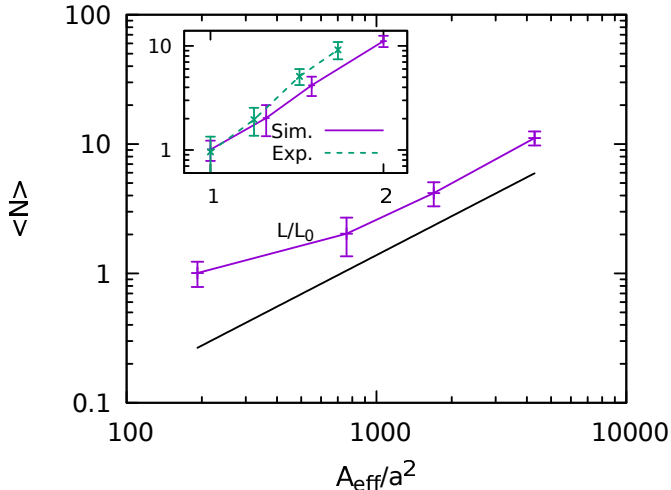


FIG. 11. Cluster number scaling against the effective nucleation area for a fixed flux $F = 5.8 \times 10^{-6}/(a^2 \Delta t)$. In the inset the number of clusters is plotted as function of L/L_0 . The error bars represent the standard deviation. The solid line represents a power law with a slope of one.

the boundary conditions only have a minor impact on the nucleation behavior? Without boundaries one would expect the simple scaling $\langle N \rangle \propto L^2$. For fixed flux values we show the relation between $\langle N \rangle$ and L in the inset of Fig. 11, both for the simulation and the experimental data. Interestingly, both data set display a similar slope in the double logarithmic representation. It is, however, larger than two. These deviations have to do with the fact that nucleation can only occur in the center of each cell. The area, where nucleation is possible, is denoted as A_{eff} . We define it as the area of a circle with the full width and half maximum (see Fig. 7) as diameter, determined for the specific values. Plotting $\langle N \rangle$ as a function of A_{eff} , indeed yields a slope of one, starting from $\langle N \rangle$ -values as small as 2. Thus, the number of clusters is extensive for

$\langle N \rangle \geq 2$ and the boundary effect is just reflected by the presence of a zone where no nucleation can take place.

IX. DISCUSSION/SUMMARY

Based on a new experimental way to generate a regular array of clusters, possibly formed by functionalized organic molecules, we have studied this boundary-induced nucleation control from a theoretical perspective. In particular we have compared the experimental data with the outcome from kinetic Monte Carlo simulations. More specifically, we have analyzed the quality of nucleation and position control, the flux vs. length-dependence to guarantee the presence of a single cluster per cell and the dependence of the number of clusters on the effective growth area. In all cases we have obtained a very good agreement between experiment and simulation. This work constitutes another example that analysis of a simple lattice model indeed captures many properties of the cluster formation of complex molecules.

Furthermore, via comparison with analytical expressions for the stationary concentration profile in the cluster-free sub-ensemble and employing key results of nucleation theory, the flux vs. length-dependence can be fully understood. It is important to mention that most properties result from surprisingly simple scaling relations. Of key importance is the proportionality of the nucleation rate and the external flux, giving rise to a universal behavior how the number of cells with one cluster increases with increasing coverage. Actually, this universality was the major ingredient to connect the analytical and the numerical/experimental pieces of information.

We hope that combined experimental and theoretical analysis of boundary-induced nucleation control and the observed generality of this approach may inspire more work along this line. Possible extensions such as the simultaneous use of different molecules are conceivable.

ACKNOWLEDGMENTS

This work was supported through the Transregional Collaborative Research Centre TRR 61 (projects B1 and B12) by the DFG.

-
- [1] S. R. Forrest, *Chem. Rev.* **97**, 1793 (1997).
 - [2] S. Pratontep, M. Brinkmann, F. Nüesch, and L. Zuppiroli, *Phys. Rev. B* **69**, 165201 (2004).
 - [3] B. Lucas, T. Trigaud, and C. Videlot-Ackermann, *Polym. Int.* **61**, 374 (2012).
 - [4] H. Yamada, T. Okujima, and N. Ono, *Chem. Commun.*, 2957 (2008).
 - [5] H. Uoyama, K. Goushi, K. Shizu, H. Nomura, and C. Adachi, *Nature* **492**, 234 (2012).
 - [6] P. Maksymovych, D. C. Sorescu, D. Dougherty, and J. T. Yates, *J. Phys. Chem. B* **109**, 22463 (2005).
 - [7] H. Glowatzki, S. Duhm, K.-F. Braun, J. P. Rabe, and N. Koch, *Phys. Rev. B* **76**, 125425 (2007).
 - [8] S. R. Wagner, R. R. Lunt, and P. Zhang, *Phys. Rev. Lett.* **110**, 086107 (2013).
 - [9] A. Pimpinelli, L. Tumbek, and A. Winkler, *J. Phys. Chem. Lett.* **5**, 995 (2014).
 - [10] W. C. Wang, D. Y. Zhong, J. Zhu, F. Kalischewski, R. F. Dou, K. Wedeking, Y. Wang, A. Heuer, H. Fuchs, G. Erker, and L. F. Chi,

- Phys. Rev. Lett. **98**, 225504 (2007).
- [11] W. Wang, C. Du, D. Zhong, M. Hirtz, Y. Wang, N. Lu, L. Wu, D. Ebeling, L. Li, H. Fuchs, and L. Chi, *Advanced Materials* **21**, 4721 (2009).
 - [12] W. Wang, C. Du, H. Bi, Y. Sun, Y. Wang, C. Mauser, E. Da Como, H. Fuchs, and L. Chi, *Advanced Materials* **22**, 2764 (2010).
 - [13] H. Wang, W. Wang, L. Li, M. Hirtz, C. G. Wang, Y. Wang, Z. Xie, H. Fuchs, and L. Chi, *Small* **10**, 3045 (2014).
 - [14] H. Wang, O. Buller, W. Wang, A. Heuer, D. Zhang, H. Fuchs, and L. Chi, *New Journal of Physics* **18**, 053006 (2016).
 - [15] L. Nurminen, A. Kuronen, and K. Kaski, *Phys. Rev. B* **63**, 035407 (2000).
 - [16] C. Lee and A.-L. Barabási, *Applied Physics Letters* **73**, 2651 (1998).
 - [17] P. Jensen, A.-L. Barabási, H. Larralde, S. Havlin, and H. E. Stanley, *Phys. Rev. B* **50**, 15316 (1994).
 - [18] A. Voter, in *Radiation Effects in Solids*, NATO Science Series, Vol. 235, edited by K. Sickafus, E. Kotomin, and B. Uberuaga (Springer Netherlands, 2007) pp. 1–23.
 - [19] S. F. Hopp and A. Heuer, *The Journal of Chemical Physics* **133**, 204101 (2010), <http://dx.doi.org/10.1063/1.3478441>.
 - [20] E. W. Forsythe, D. C. Morton, C. W. Tang, and Y. Gao, *App. Phys. Lett.* **73**, 1457 (1998).
 - [21] F. Lied, T. Mues, W. Wang, L. Chi, and A. Heuer, *The Journal of Chemical Physics* **136**, 024704 (2012).
 - [22] N. Metropolis, A. W. Rosenbluth, M. N. Rosenbluth, A. H. Teller, and E. Teller, *J. Chem. Phys.* **21**, 1087 (1953).
 - [23] T. Michely and J. Krug, *Islands, Mounds and Atoms* (Springer-Verlag Berlin Heidelberg, 2004).
 - [24] W. K. Burton, N. Cabrera, and F. C. Frank, *Philosophical Transactions of the Royal Society of London A: Mathematical and Physical Sciences* **237**, 399 (1971).
 - [25] A. K. Myers-Beaghton and D. D. Vvedensky, *Phys. Rev. B* **42**, 5544 (1990).
 - [26] F. Kalischewski, J. Zhu, and A. Heuer, *Phys. Rev. B* **78**, 155401 (2008).
 - [27] B. Rangelov, M. S. Altman, and I. Markov, *Phys. Rev. B* **75**, 245419 (2007).
 - [28] J. Venables, G. Spiller, and M. Hanbucken, *Reports on Progress in Physics* **47**, 399 (1984).
 - [29] J. G. Amar and F. Family, *Phys. Rev. Lett.* **74**, 2066 (1995).